EXPERIMENTAL AND NUMERICAL MODELLING OF COASTAL PROCESSES

William Booker, Thomas Goodfellow and Jacob van Alwon

1. ABSTRACT

An experimental wave tank was used to model overtopping on coastal defence structures with the aim of designing a new tank to be used for educational purposes by JBA Trust. Smoothed Particle Hydrodynamics and Finite Element Methods were used to model the tank numerically; verified analytically using shallow water wave theory. SPH simulations gave good agreement with experimental free surface profiles, but overtopping calculations required further study.

Keywords - Coastal Defence, SPH, Finite Element

2. INTRODUCTION

Coastal structures must be designed such that under severe wave conditions the amount of water making it onto land is minimised. Prediction of this 'overtopping' is important when designing defences and has been the subject of much research worldwide (see Tsuruta and Goda [1968], Owen [1980] and Goda [2010]). JBA Group is an environmental, engineering and risk group who work actively in the area of coastal risk management. A not-for-profit subsidiary, JBA Trust, work to support and promote scientific research, education and outreach in this area [JBA, 2015].

2.1. Aims and Objectives

JBA Trust proposed a project to design and build a model wave tank which could demonstrate the effect of coastal defence structures on the overtopping of water waves. The aim of the project was to test different wave makers and coastal defences in an experimental tank and use the findings to inform the design of a new tank to be manufactured by a local modelling consultancy, HydroTec [HydroTec, 2015].

Objectives included the design and production of the tank, wavemaker and defences along with numerical simulations of the free surface and overtopping discharges using Smoothed Particle Hydrodynamics (SPH) and Finite Element Methods (FEM). Analytical solutions were used to evaluate the numerical simulations, subsequently comparing them with results obtained from experiment.

3. METHOD

The wave tank was required to fit inside a particular vehicle for transportation, so the length was limited to 1.5 m. Therefore the experimental tank was blocked off at 1.5 m using modelling foam which could be wedged in and sealed with weatherproof tape. The tank dimensions were thus $200 \times 183 \times 1500$ mm^3.

3.1. Scaling

As in many coastal engineering problems, horizontal length scales are much larger than vertical length scales. If the model was scaled directly in the tank, water depths would be on the order of a few millimetres at which surface tension dominated capillary waves form. In order to create a visually representative tool a geometrically distorted model was required. Wave conditions were found empirically to provide a good visual tool and were scaled up using a wavelength equation arising from linear theory as described by Hughes [1993].

$$\frac{\lambda_p}{\lambda_m} = \left(\frac{T_p}{T_m}\right)^2 \frac{tanh\left(\frac{2\pi h_p}{\lambda_p}\right)}{tanh\left(\frac{2\pi h_m}{\lambda_m}\right)}, \qquad (1)$$

where λ is the wavelength, T is the period and h is the water depth. A scaling factor was introduced, $N_x = x_p/x_m$ where x_p is parameter in prototype and x_m is a parameter in the model. Rewriting (1) in terms of scaling factors then as wavelength $>>$ depth, tanh functions approach their arguments and the relation can be expressed as

$$N_\lambda = \sqrt{N_h} N_T. \qquad (2)$$

Another criterion used to evaluate similitude was a modified Froude number given by,

$$F_c = \frac{c}{\sqrt{g\lambda}}, \qquad (3)$$

which expresses the ratio of full wave speed to the shallow wave speed. Note wave speed, c was used in place of fluid speed as this is more relevant to wave motion analysis.

A water depth of 70 mm was found to be appropriate to avoid capillary waves while a wavelength of 1m and period of 1.25 s provided a good

levels of overtopping. These parameters were scaled using equations (2) and (3) and compared to conditions around the British coast. The wavelength scaling factors calculated directly appeared to be in agreement with that calculated using equation (2), with a difference of 1.11%.

3.2. Wave Generation

One of the aims of the project was to design and build a wavemaker capable of reliably producing the required conditions for wave overtopping in the tank. A number of concepts were explored before deciding on a final design. It was important to investigate the physics behind waves and how they are commonly generated in scale models.

Linear deep water waves typically exhibit circular particle motion with the radius reducing towards the bed. On the other hand the particle motion is elliptical in shallow water due to the effects of the bottom surface [Hofmann, 2008]. An articulating flap is a common method of generating waves, where a paddle hinged at the bottom would approximate circular motion as suited to deep water waves, and a piston would approximate elliptical motion as suited to shallow water waves [Edinburgh Designs, 2015]

The wave tank was designed to model shallow water processes, so a paddle hinged at the bottom would be unsuitable. Indeed such a wavemaker was tested and found to provide low amplitude waves resulting in zero discharge. Manufacturing limitations prohibited the production of a piston-type wavemaker, so a paddle hinged above the free surface was designed and manufactured. This wavemaker went through a number of design iterations, improving the mechanical linkage between a motor and the paddle. The penultimate design is shown in Figure 1 – an improved version avoids the need for an inefficient pulley system by fixing a motor with a higher gear ratio directly to the shaft.

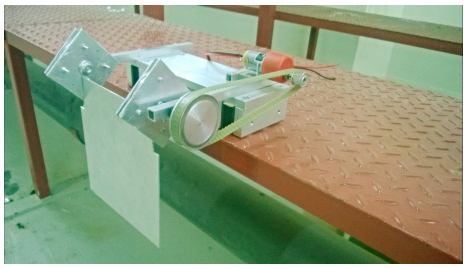

Figure 1: Penultimate wavemaker design.

The motor was controlled using an Arduino Uno micro-controller. Wave conditions were controlled by modifying the program and it was possible to move the paddle continuously, produce a standing wave or send a single wave down the tank. A square wave (on/off) signal was used to control the motor. A sinusoidal signal was also tested but was unable to produce required overtopping and provided no real benefit over a square wave.

A rotary optical encoder was used to record the angle of the paddle over time. It was found that after a number of experiments the paddle position needed to be recalibrated as reflected waves pushed the paddle backwards, though the effect on wave conditions was negligible. Furthermore encoder readings showed that the paddle experienced a short acceleration period before reaching full velocity. Overall the wavemaker reliably produced he required waves and experiments were highly repeatable.

3.3. Coastal Defences

Coastal defences are primarily required to reduce or eliminate the overtopping of water to prevent flooding in surrounding areas, though they may also be required to prevent erosion and scouring of beaches. Vertical walls can provide flood protection, however, reflected waves may cause a deterioration in conditions seaward of the wall [Thomas and Hall, 1992]. Spray can also be an issue with vertical walls impacted by high energy waves.

Energy can be dissipated with sloping walls, steps or rock defences, each case having distinct advantages and disadvantages. For instance a sloped structure may increase ‘green-water’ overtopping where a sheet of water is ejected over the structure, whereas turbulence from steps and rubble may cause spray. Re-curve or wave return walls may also be used to deflect any up-rushing water seaward. To show how defences *reduced* overtopping for a given wave condition a range of defences were tested. These were: A vertical wall, 1:2 slope, 1:3 slope, 1:3 stepped slope and re-curve as shown in the schematic in Figure 2.

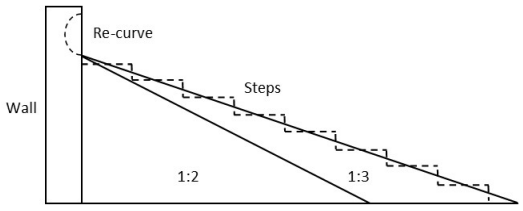

Figure 2: Coastal defences schematic.

Coastal defences were manufactured using modelling foam as this was easy to shape and offered a tight fit within the tank to prevent floating. The dimensions of defences used in experiments are

shown in Appendix A.

3.4. Analytic Solution

Linear wave theory provided initial insight into the problem and was used to evaluate the numerical codes. The set of analytical equations describing the motion were obtained by considering conservation of mass in a system with constant density, resulting in the continuity equation:

$$\nabla.\mathbf{v} = 0,$$

where **v** is the velocity field. If the flow is irrotational the velocity can be expressed as the gradient of a scalar field, ϕ, known as the potential velocity. This results in the Laplace equation,

$$\nabla^2\phi = 0.$$

Seeking separable solutions of the form

$$\phi = F(x)G(z)e^{-i\omega t},$$

yielded the analytical solutions for the unforced velocity potential and free surface.

$$\begin{aligned} \phi &= A\cos\kappa x\cosh\kappa(z+H_0)e^{-i\omega t}, \\ \eta &= B\cos\kappa x\cosh\kappa H_0\sin\omega t, \end{aligned} \tag{4}$$

where A and B are complex consants, H_0 is the depth of fluid, ω is the frequency and κ is the wavenumber. Enforcing a solid wall boundary condition at the end of the tank, the wavenumber was found to be quantized by $\kappa = m\pi/L$ for integer m. These are the natural frequencies in the tank, forcing at this frequency would produce resonant standing waves. The free-surface boundary conditions were then used to obtain the dispersion relation

$$\omega^2 = g\kappa\tanh(\kappa H_0). \tag{5}$$

3.5. Smoothed Particle Hydrodynamics

Smoothed particle hydrodynamics is a meshless method of simulating fluid motion using a Lagrangian solver on a set of particles. It is well suited to modelling free surface problems, particularly those involving fluid structure interaction [Gomez-Gesteira et al., 2010]. Navier-Stokes equations are integrated based on properties of particles within a 'smoothing length', h of the particle in question. A kernel, or smoothing function is used to define this length. A full description of the equations and references is found in Gomez-Gesteira et al. [2012]. Calculations are not performed in empty areas which has the potential to speed up calculations. However, due to the large number of particles required for some simulations, times can be significantly longer than for mesh-based methods.

3.5.1. Verification

Test cases based on the analytic solutions for linear waves in a tank were evaluated in open-source SPH software DualSPHysics to determine its viability. It was known from previous studies that the code performed well when modelling wave breaking [Dalrymple and Rogers, 2006], dam-break behaviour [Crespo et al., 2008] and wave-structure interaction [Gomez-Gesteira and Dalrymple, 2004]. However numerical damping in the system was known to affect wave propagation.

The first step in checking the simulations was to determine particle independence. This was performed by forcing waves using a rotary paddle, as used in the experiments, and reducing the distance between particles until the solution no longer varied significantly. The study showed that a particle spacing of 2 mm was a reasonable compromise between accuracy and computational speed for our wave tank simulations.

The particle independence study showed compressible behaviour in that the fluid volume was changing over the course of the simulation. DualSPHYsics modells the fluid as weakly compressible, relating the speed of sound in the fluid to the pressure and density with Tait's equation

$$P = B\left[\left(\frac{\rho}{\rho_0}\right)^{\gamma} - 1\right], \tag{6}$$

where $B = c_0^2\rho_0/\gamma$ and c_0 is the speed of sound at reference density. It was required to choose a speed of sound to produce incompressible behaviour. A sensitivity study was performed which looked at the evolution of the free surface height of water at rest in a tank with no wavemaker. The change in volume was minimal at a sound speed of 20.5 m/s, whereas speeds above this caused the volume to increase and speeds below caused it to decrease. This was verified by comparing the pressure and density in the fluid to that obtained using hydrostatic balance. Equation (6) was integrated over the domain to give an expression for pressure in terms of atmospheric pressure, p_a and reference density, ρ_0:

$$p = B\left[\left(1+\frac{p_a}{B}\right)^{\frac{\gamma-1}{\gamma}} - \left(\frac{\gamma-1}{\gamma}\right)\frac{\rho_0 g z}{B}\right]^{\frac{\gamma}{\gamma-1}} - B.$$

Equation (6) was rearranged to give density as

$$\rho = \rho_0\left(1+\frac{p}{B}\right)^{\gamma-1}.$$

Comparison of results to those obtained using the above equations showed there was little difference at 20.5 m/s suggesting that this solution was in relative hydrostatic balance.

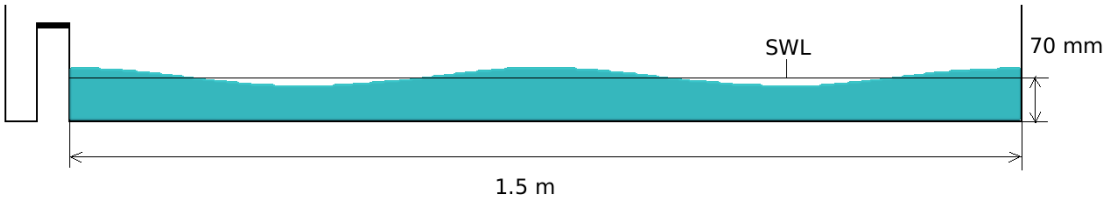

Figure 3: Initial conditions for damping test.

The position of the free surface at zero velocity was set as an initial condition in DualSPHysics to evaluate the level of damping. Zero velocity was known to occur at maximum displacement, where potential energy was maximum and kinetic energy was minimum. Equation (4) was used to obtain this free surface height and import it into DualSPHysics as a .STL file. This is shown in Figure 3. The simulation was set to run with no forcing and the free surface height was integrated to give the potential energy as

$$PE = \frac{1}{2}\left(\int_0^L \eta^2\right), \tag{7}$$

where η is fluid displacement from rest. The energy after each period – i.e. maximum displacement – was recorded and plotted for different particle spacing as shown in Figure 4.

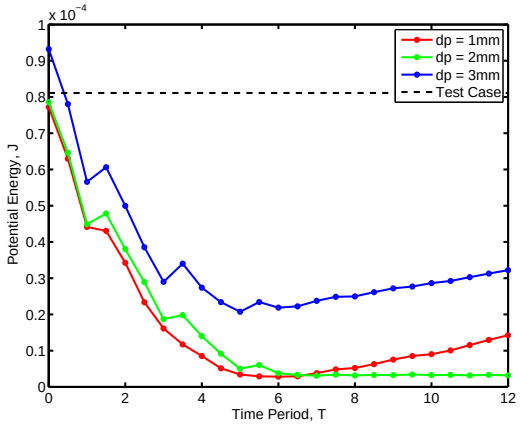

Figure 4: Comparison of energy loss over time for different particle spacing.

After coming to rest at around 5 periods the energy began to diverge for 1 and 5 mm cases, whereas 2 mm remained constant. This was because the speed of sound had been determined for a particle spacing of 2 mm and so the fluid volume remained constant due to hydrostatic balance. Conversely, the volume continued to change when the fluid was at rest for other particle distances. This indicated that particle spacing as well as the speed of sound had an effect on compressibility. Furthermore the free-surface in the 5 mm case was higher throughout the simulation, most likely due to a larger kernel smoothing length resulting in extra mass recorded above the free-surface particles.

Regardless, the rate of energy loss was similar in each case, levelling out after roughly 5 periods. The analytical solution showed no change in energy as expected. The L2-norm was used to evaluate the error between SPH simulations and the analytical solution from 0 to 6 Periods – before solutions began to diverge. The L2-norm was 2.929 for 1mm, 2.957 for 2mm and 2.208 for 5mm; the difference in values being due to the initial height as discussed. The rate of damping was seen to be consistent in that energy reduced by half over two wave periods. This was of initial concern when performing simulations and was to be taken into account when analysing results.

3.6. Finite Element Method

The fluid motion was modelled using the shallow water equations, so it was assumed that the fluid motion was depth and width independent, with the latter assumption being true in the case for the SPH simulations.

$$\begin{aligned} \frac{\partial}{\partial t}(h) + \frac{\partial}{\partial x}(hu) &= 0, \\ \frac{\partial}{\partial t}(u) + \frac{\partial}{\partial x}(\frac{1}{2}u^2 + gh) &= -g\frac{db}{dx}, \end{aligned} \tag{8}$$

where h is the fluid height, u is the velocity in the x direction, g is gravitational body force and b is the basal topography.

The numerical flux chosen was the Lax-Friedrichs flux, which is an approximate linear Riemann solver and the timestepping was a 2nd order total variational diminishing Runge-Kutta method (RK-TVD). The RK-TVD method was preferred because it has the property of bounding the growth of spurious oscillations that can occur when numerically simulating discontinuous solutions such as breaking waves. A second order method

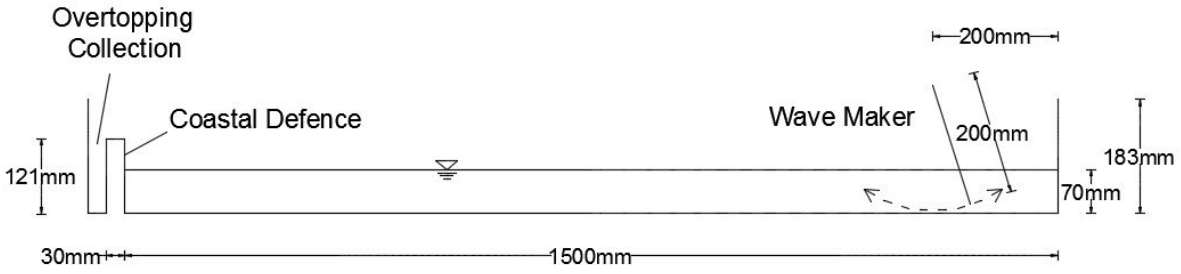

Figure 5: Experimental arrangement schematic.

was chosen as the RK-TVD scheme must be at least one order higher than the order of the polynomial basis [Cockburn and C.W., 1989]. The wavemaker boundary condition was approximated as a piston wavemaker with a sinusoidal motion, this can be implemented as

$$u_{x=0} = \alpha\sigma cos\sigma t, \tag{9}$$

where α, σ are the wavemaker's amplitude and frequency respectively. This lead to the computational domain subsequently being 1.3m, so the tank was simulated from the initial rest position of the wavemaker to the beginning of the sea wall.

As the governing equations were depth independent, there was no natural way to measure overtopping. This was subsequently implemented as a timestepper correction at the stationary wall boundary condition:

$$\text{if } h_{\text{sea wall}} \geq 0.12$$

$$\implies q = q + h_{\text{sea wall}} - 0.12$$
$$\text{and } h_{\text{sea wall}} = 0.12,$$

where q is the measured height of overtopping discharge. This was compared to the volumes in the experiments by multiplying by tank width and element width. Modelling the overtopping as such resulted in the assumption that any fluid higher than the sea wall overtopped, therefore it was not possible to model the re-curve coastal defence accurately. Also the basal topography term assumed that the tank floor was continuous meaning that this method was not appropriate for modelling the stepped coastal defence.

3.7. Experimental Procedure

Experiments were performed in the tank of $200 \times 183 \times 1500$ mm^3. The wave maker paddle was located at 1300 mm from the coastal defence. A schematic of the arrangement is shown in Figure 5 and an image of the tank is shown in Appendix B.

3.7.1. Wave Conditions

The coastal defences tested are shown in Appendix A. Each defence was tested under continuous wave conditions and then with a single wave. Initial tests were performed to determine a period and wavelength which produced reasonable levels of overtopping. To avoid producing standing waves the wavenumber, $\kappa = m\pi/L$ was chosen using a non-integer value of m. A value of m = 1.5 was used with L = 1.3 m, producing a wavelength and period calculated using equation (5) as shown in Table 1. The amplitude was set by changing the voltage delivered to the motor until the desired overtopping was achieved with a vertical wall. This is because the height of the coastal defence was fixed, however it could be changed to accommodate smaller waves. These conditions were used to send a single wave down the tank, while a standing wave was produced with m = 4, an integer. The amplitude was reduced because overtopping was not desired; of more interest was increase in wave height over time.

Table 1: Wave conditions used in experiments.

Wave Type	Wavelength, λ (m)	Period, T (s)
Continuous	1.005	1.25
Single	1.005	1.25
Standing	0.650	0.84

3.7.2. Measurements

Measurements were taken of the quantity of overtopped water after 15 wave periods for each coastal defence. Experiments were repeated three times for continuous waves and five times for single waves. This is because overtopping was much less in the single case and so there was more chance of variability. Volume was measured by catching water in a bucket and decanting it into a measuring cylinder. This allowed the discharge (m^3s^{-1}) to be calculated and also a direct comparison of overtopping for each structure.

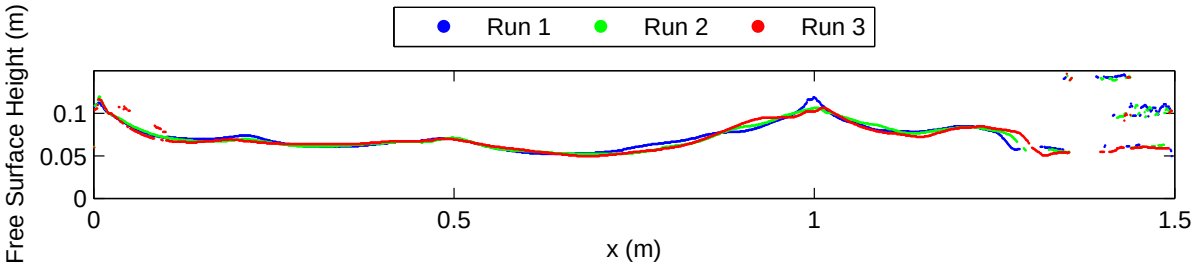

Figure 6: Free surface of waves impacting 12mm high vertical wall at 17.8 s for three experimental runs.

The free surface was monitored by employing image analysis on a video of each experiment. The back wall of the tank was lined with white plastic and food dye was used to colour the water black. This produced a good contrast which aided in extracting the free surface. The program assigned either a 1 or 0 to each pixel in the image depending on whether it was light or dark. Using Matlab, the boundary between 0s and 1s could then be identified as the free surface.

3.7.3. Experimental Error

Sources of possible error included a leakage of water past the coastal defence as it was not entirely sealed. This was measured at 1.25 ml/s which equated to approximately 23 ml over the course of 15 wave periods. However this value was highly variable depending on coastal defence used, so was not subtracted from final measurements. It was instead reasoned that the average leakage was the same in each case and so comparisons were made directly.

The foam structures were buoyant and despite being secured to the base of the wave tank they were lifted by approximately 5 mm. Therefore the defence was slightly higher and water filled in the small gaps beneath and to the sides of the defence. Finally the paddle experienced a short period of acceleration before reaching full speed which would not be seen in SPH simulations.

4. RESULTS

Results of experiments and simulations are presented here and discussed in section 5. It was important to determine the repeatability of experiments, therefore a plot was produced showing the free surface of a continuous wave impacting the vertical wall after running for a set time. Figure 6 shows the free surface of three runs, each at 17.8s. The anomalous data behind the wave maker on the right-hand side was due to shadows captured in image processing.

The mean volume of overtopping recorded in the continuous wave experiment is provided, along with that from simulations in Table 2.

Table 2: Overtopping of water in experiments and simulations.

	Mean Overtopping (ml)	
Defence	Experiment	SPH
Vertical Wall	502	26.5
Recurve	48	24.8
1:2 Slope	415	0
1:3 Slope	431	0
Steps	48	0

Images of the overtopping of a single wave on different structures were collected in Figure 7. These close-ups of overtopping pattern were useful in explaining values observed in Table 2. It was required to know the degree of similarity between the free surface profiles observed in experiments and those obtained in SPH simulations. Figure 8 shows a comparison of results obtained at a time of 11.5s for continuous waves impacting a vertical wall, with: a) showing the SPH output and free surface height, b) showing a frame of the recorded video of the experiment and c) comparing the free surface heights from both.

It was also important to observe for how long the experimental and SPH free-surfaces matched. This was achieved by plotting the curves against each other at a time of 2.7s and then again at 178s as shown in Figure 9 for a stepped structure. It was also of interest to monitor the free surface in the experiment for a standing wave to see how it compared to the SPH simulation. Figure 10 shows a comparison of surface height at a point in the centre of the tank for a standing wave. Perhaps a more descriptive plot is shown in Figure 11 of the change in potential energy over time along with the peak potential energy for the SPH simulation. However this was only available for the SPH simulation due to time limitations, so no direct comparison can be made with experiment.

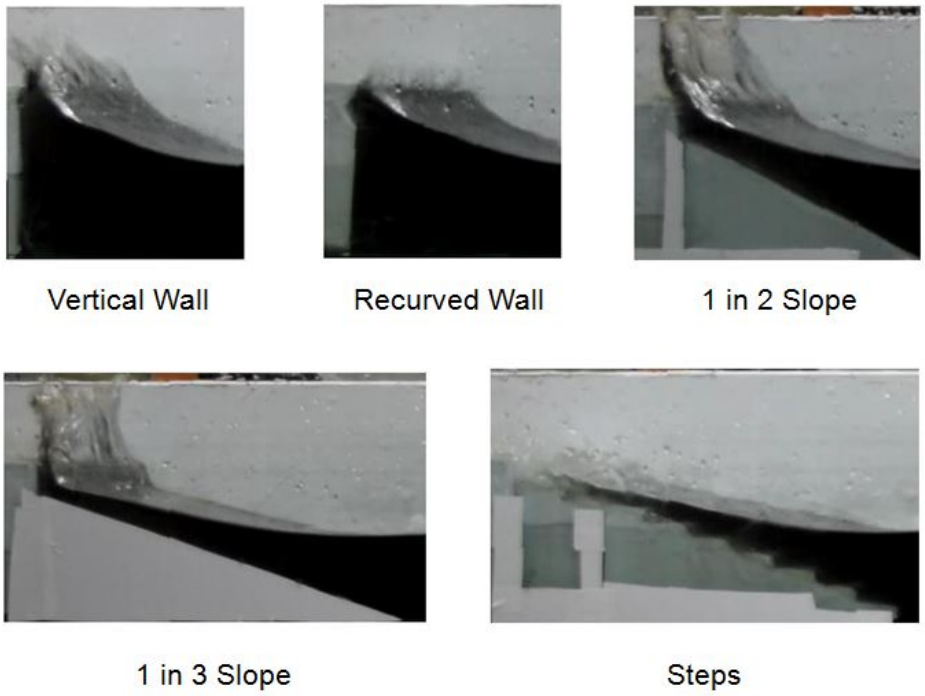

Figure 7: Images of Overtopping for Each Coastal Defence.

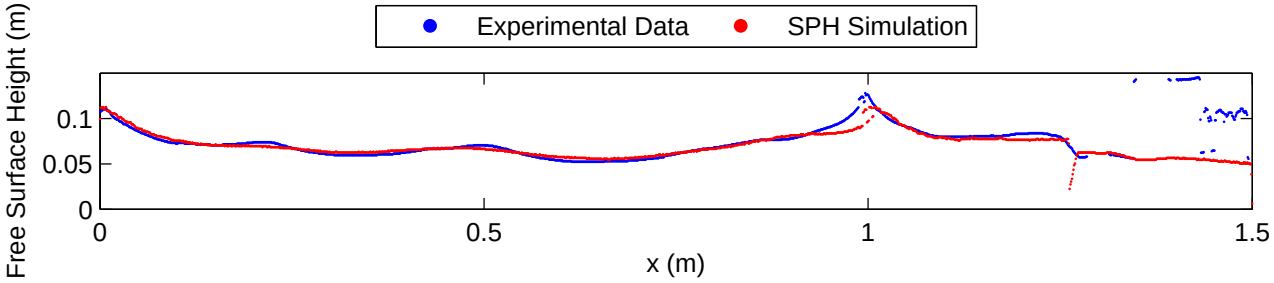

(a) Free Surface Plot

(b) Camera Image

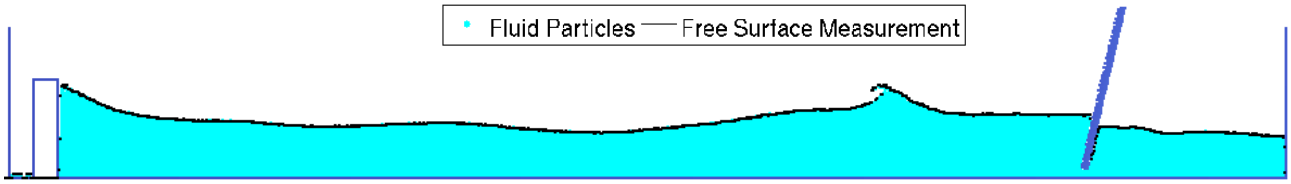

(c) SPH Visualisation

Figure 8: Experimental and numerical free surface profiles for a vertical wall after 11.5 seconds.

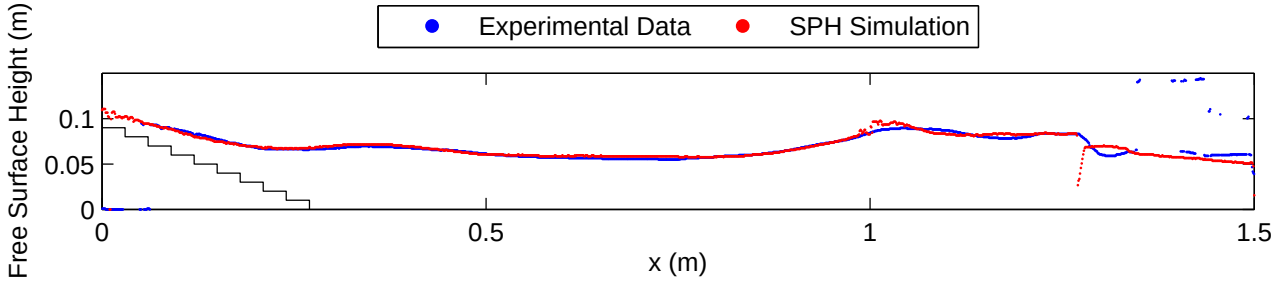

(a) t = 2.7 s

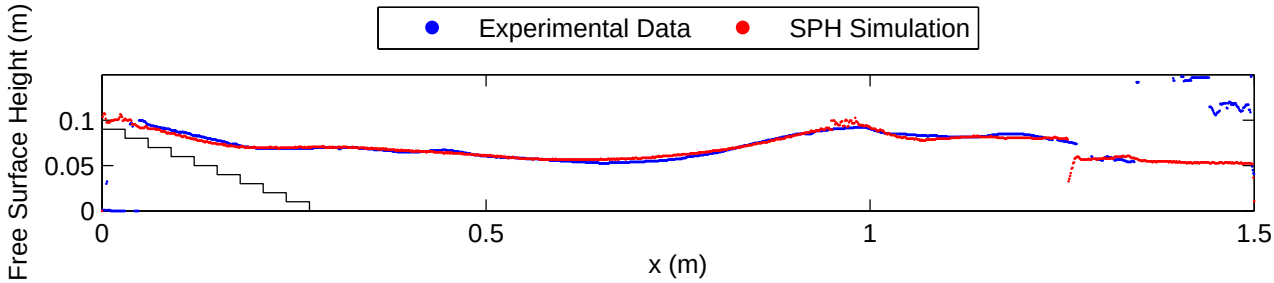

(b) t = 17.8 s

Figure 9: Change in solutions over time.

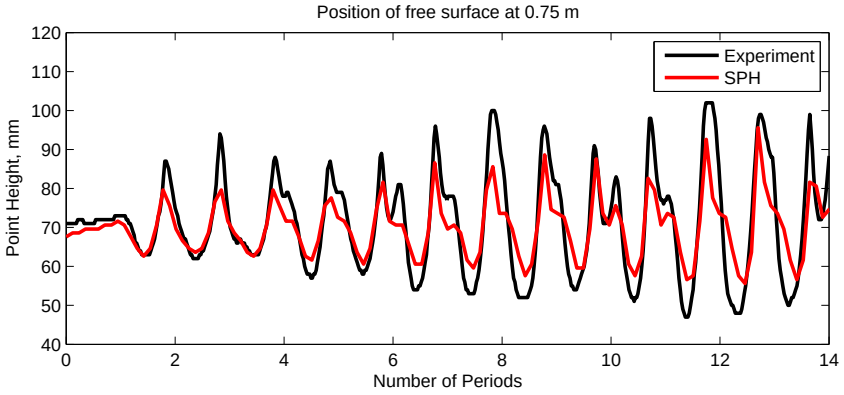

Figure 10: Height of a single point over time for standing wave.

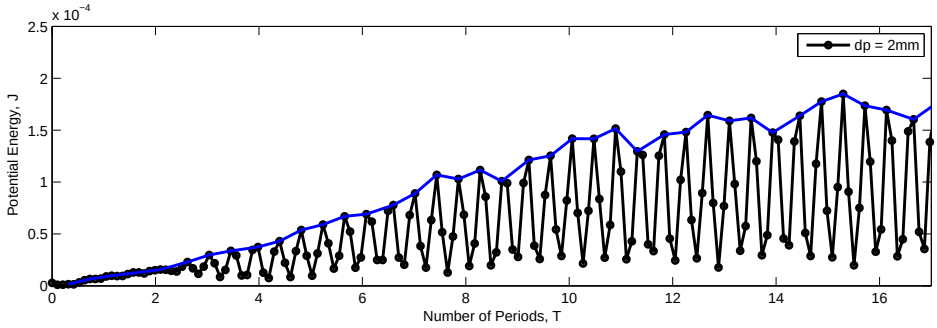

Figure 11: Energy change in a standing wave produced with SPH.

5. DISCUSSION

The experiments were observed to be largely repeatable. Figure 6 showed that free surface profiles were very much the same after 17.8 seconds, or approximately 15 wave periods. This was also observed for other coastal defences, suggesting that in the experiments the wave conditions produced were consistent between experiments.

Experimental and numerical overtopping on different structures was presented in Table 2. The FEM code did not produce any sensible results, thought to be due to an incorrect approach used, therefore results are not included here. In the experiments a vertical wall exhibited the most overtopping at 502 ml. Using either a recurve or a stepped slope reduced this significantly to 48 ml. Using a 1:2 slope and 1:3 slope reduced the overtopping to 415 ml and 431 ml respectively; a less significant reduction to that obtained with steps or recurve. There was little difference between the overtopping from either slope, though the 1:2 slope produced slightly less than the 1:3. The splash patterns shown in Figure 7 helped to demonstrate why different overtopping amounts were observed. It could be seen that the recurve deflected any water seaward while the steps absorbed the majority of the wave energy. However the slope acted as a ramp, producing a large amount of 'green water' overtopping as described in Section 3.3. In contrast the impact of a wave with the vertical wall caused a significant splash and run-up of water. However it was expected that the slope would produce more overtopping [HR Wallingford, 2007] than the vertical wall which was not observed. A possible reason was that the approaching waves had broken due to reflected waves, effectively reducing energy sufficiently for the slopes to dissipate energy efficiently.

The overtopping predicted with SPH simulations was significantly less than that observed experimentally, with zero overtopping calculated for the slopes and steps in SPH. The error in SPH simulations may have been due to the damping present in the system, or the particle spacing may have been too coarse to accurately represent flow *around* the structure. Another reason could have been the choice of viscosity value used in simulations. If the viscosity was too low then fluid may break up into droplets rather than remain as a continuous body. If it was too high the fluid may not have broken up at all. A further study would be required to vary these parameters and observe the effects.

A comparison of the free surface profile from an experiment and corresponding SPH simulation was shown in Figure 8. It could be seen that after 11.5 seconds the free surface profiles closely matched. At x = 1 m both the experiment and SPH simulation captured the wave breaking, and though SPH was in phase it did underestimate the height. Furthermore more the intermediate waves observed between x = 0 and x = 1 were more pronounced in the experiment. The reason for the low breaking wave height and smaller intermediate waves was likely due to the significant damping present in the simulations.

It was predicted that due to turbulent energy dissipation on the stepped slope, the experimental and SPH data may differ over time due to different amounts of wave absorption. However Figure 9 showed that the wave profiles were largely identical at 2.7 seconds and 17.8 s (12 wave periods later). SPH was therefore reasoned to be an accurate tool for predicting free surface profiles, though not for overtopping. Further study into calculating overtopping with SPH is warranted.

Figure 10 showed that the damping in the SPH simulations resulted in a slower growth of oscillations than in the experiment, though the waves remained in phase. The intermediate peaks were likely because the position of the measurements was not directly on a standing wave node. Figure 11 showed that the energy gradually increased in the SPH simulation before levelling off at approximately 15 periods. Again, the damping was thought to have limited the energy increase.

6. CONCLUSIONS

Experiments performed in the wave tank were found to be highly repeatable, with the wavemaker reliably generating the same wave conditions each time. Furthermore changing the coastal defences also changed the amount of overtopping as required. It would therefore be acceptable to use the tank as a visual tool for demonstrating coastal engineering practices. SPH simulations accurately captured the free-surface profile for all defences up to a time of 15 wave periods. However it significantly under-predicted the amount of overtopping which would warrant further study into the reasons why.

The tests performed in the tank helped to inform the final design of a new tank to be manufactured by HydroTec and delivered to JBA. The tank will use the same motor, drive mechanism and control mechanism but improvements to general useability will be made by HydroTec. This includes adding a tap to siphon water, switches to control wave conditions and coastal defences which can be removed and changed with ease. The final concepts are included in Appendix C.

References

B Cockburn and Shu C.W. Tvb runge-kutta local projection discontinuous galerkin finite element method for conservation laws ii: General framework. *Math. Comp. vol. 51, pp. 411-435*, 1989.

A.J.C. Crespo, Gomez-Gesteira. M., and R.A. Dalrymple. Modeling dam break behaviour over a wet bed by a sph technique. *Journal of Waterway, Port, Coastal, and Ocean Engineering, 134(6)*, 2008.

R.A Dalrymple and B.D. Rogers. Numerical modeling of water waves with the sph method. *Coastal Engineering, 53*, 2006.

Edinburgh Designs. *Wave Generators*. http://www.edesign.co.uk/waves/some-wave-1/, 2015.

Yoshimi Goda. *Random Seas and Design of Maritime Structures*. World Scientific Publishing Co. Pte. Ltd., Singapore, 2010.

M Gomez-Gesteira and R.A. Dalrymple. Using a 3d sph method for wave impact on tall structure. *Journal of Waterway, Port, Coastal, and Ocean Engineering, 130(2)*, 2004.

M Gomez-Gesteira, B.D. Rogers, and A.J.C. Crespo. State-of-the-art of classical sph for free-surface flows. *Journal of Hydraulic Research, 48 Extra Issue*, 2010.

M Gomez-Gesteira, B.D. Rogers, A.J.C. Crespo, R.A. Dalrymple, M. Narayanaswamy, and J.M Dominguez. Sphysics - development of a free-surface fluid solver - part 1: Theory and formulations. *Computers and Geosciences*, 2012.

Hilmar Hofmann. *Characteristics and Implications of Surface Gravity Waves in the Littoral Zone of a Large Lake*. Cuvillier Verlag Göttingen, Germany, 2008.

HR Wallingford. *EurOtop, Wave Overtopping of Sea Defenses and Related Structures: Assessment Manual*. Boyens Medien GmbH & Co., Holstein, Germany, 2007.

Stephen A. Hughes. *Physical Models and Laboratory Techniques in Coastal Engineering*. World Scientific Publishing Co., Massecheusets, USA, 1993.

HydroTec. *Homepage*. url: http://www.hydrotecltd.co.uk/, accessed: 2015-17-06, 2015.

JBA. *Homepage*. url: http://www.jbatrust.org/ accessed: 2015-06-08, 2015.

James Lighthill. *Waves in Fluids*. Cambridge University Press, Camrbidge, UK, 1978.

M.W. Owen. Design of seawalls allowing for wave overtopping. *HR Wallingford Report*, 1980.

R.S. Thomas and B. Hall. *Seawall Design*. Butterworth HeinemannLtd., Oxford, UK, 1992.

Senri Tsuruta and Yoshimi Goda. Expected discharge of irregular wave overtopping. In *Hydraulics Division, Port and Harbour Research Institute*, Tokyo, Japan, 1968.

A. COASTAL DEFENCES

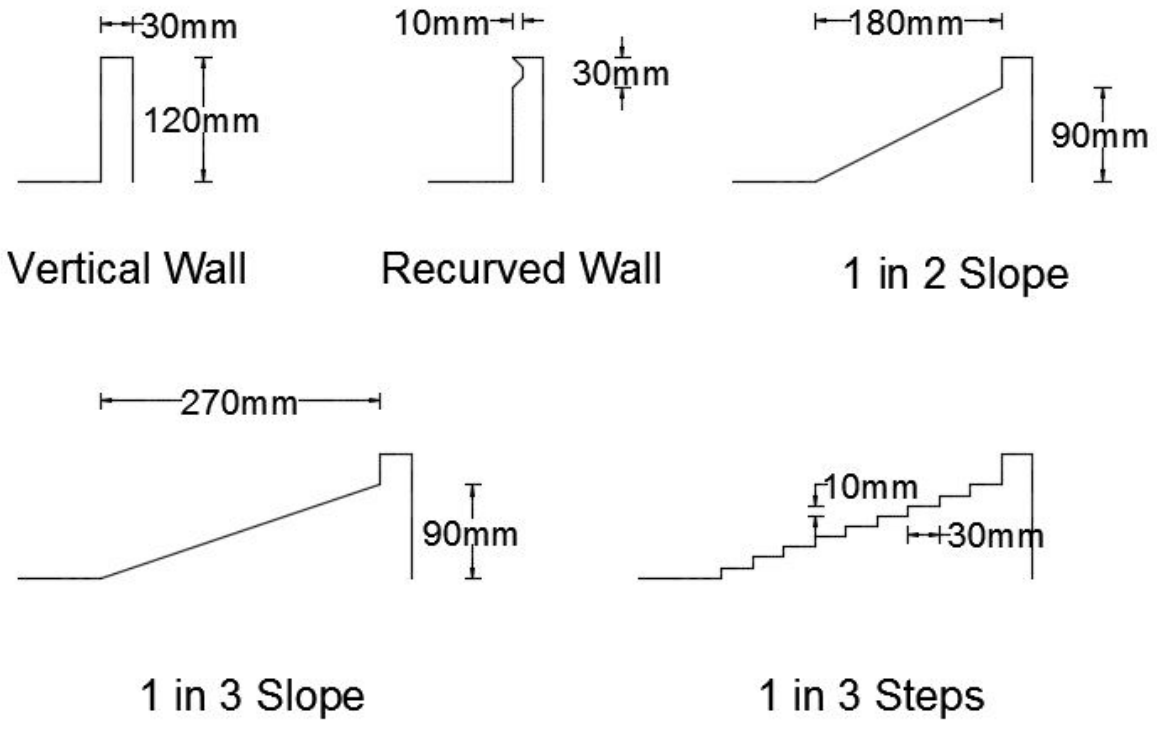

Figure 12: Coastal defences used in experiments along with dimensions.

B. WAVE TANK

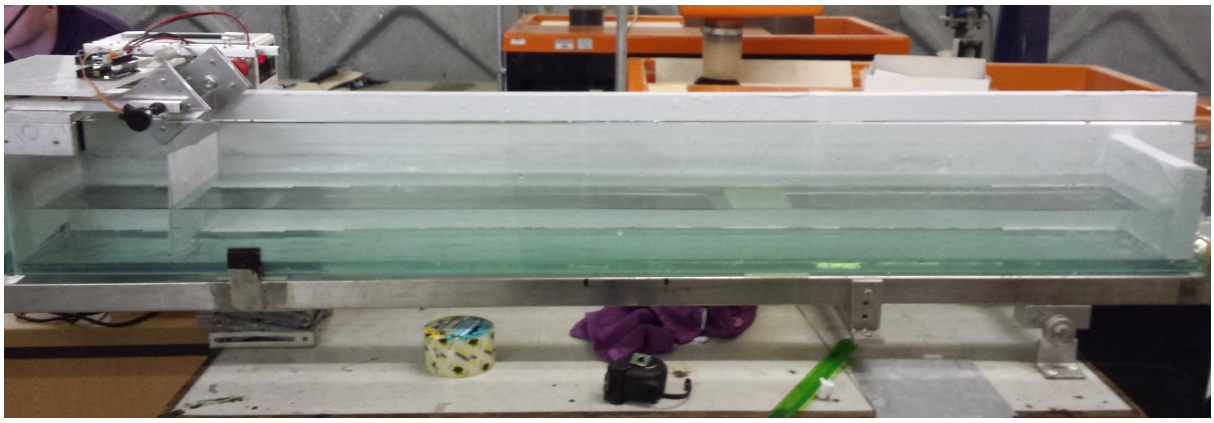

Figure 13: Image of the wave tank setup without food dye.

C. FINAL CONCEPTS

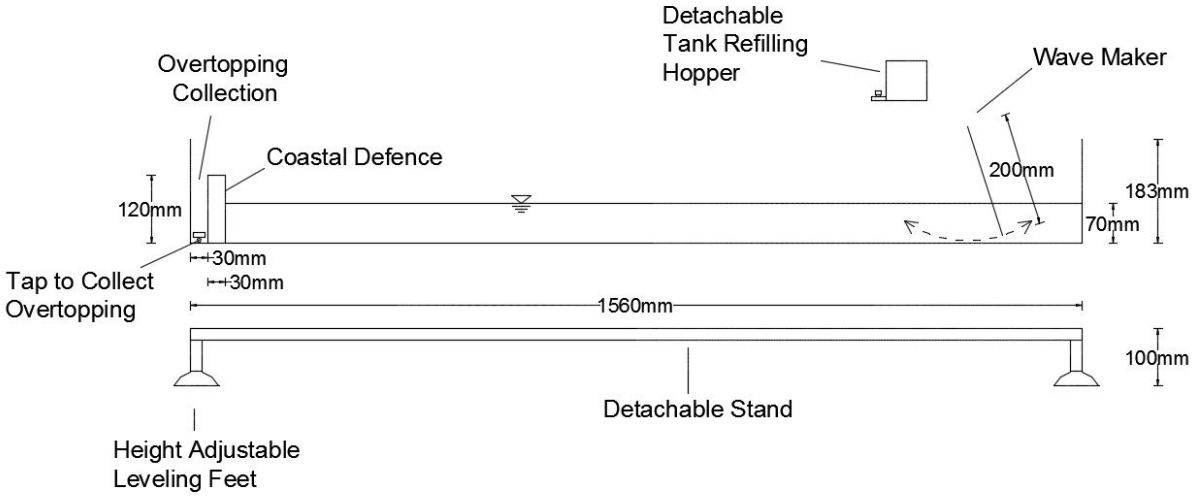

Figure 14: Final tank design with extra functionality.

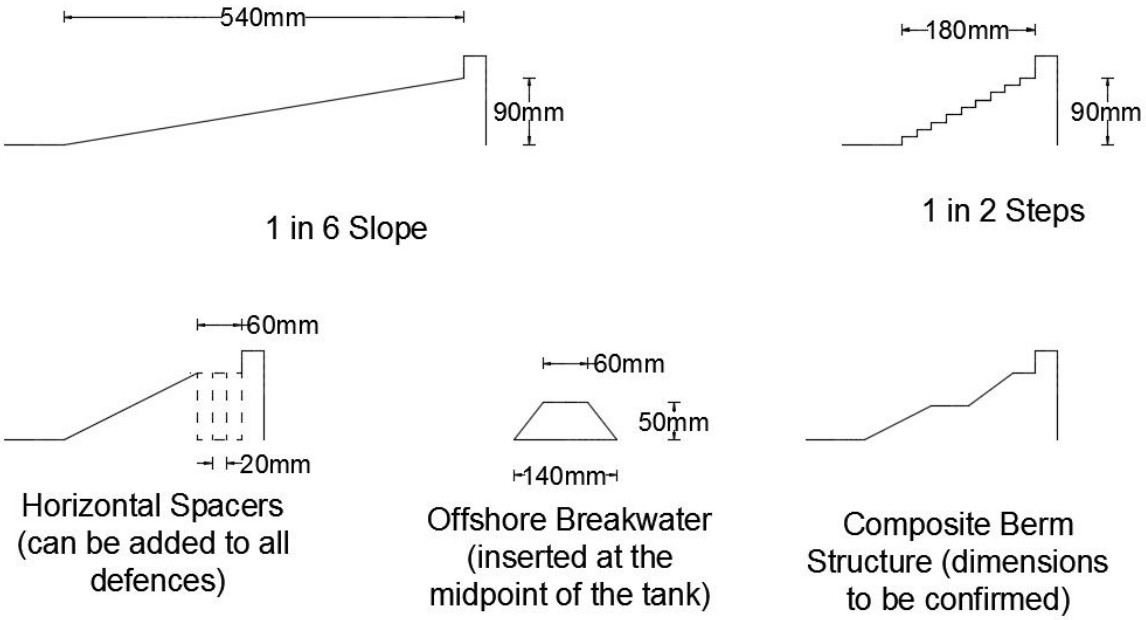

Figure 15: Additional defences to be built for JBA.